The Astrophysical Journal, 926:39 (5pp), 2022 February 10 https://doi.org/10.3847/1538-4357/ac49f0

Visible Opacity of M Dwarfs and Hot Jupiters: The TiO $B^3\Pi - X^3\Delta$ Band System

W. Doug Cameron[1] and Peter Bernath[1,2]
[1] Department of Physics, Old Dominion University, Norfolk, VA, 23529, USA; wcame002@odu.edu
[2] Department of Chemistry and Biochemistry, Old Dominion University, Norfolk, VA, 23529, USA
Received 2021 October 27; revised 2021 December 8; accepted 2022 January 5; published 2022 February 10

Abstract

The TiO $B^3\Pi - X^3\Delta$ electronic transition (γ' system) is an important opacity source in the atmospheres of M dwarfs and hot Jupiter exoplanets. The 0–0, 1–0, and 2–1 bands of the $B^3\Pi - X^3\Delta$ band system have been analyzed using a TiO emission spectrum recorded at the McMath-Pierce Solar Telescope, operated by the National Solar Observatory at Kitt Peak, Arizona. Improved spectroscopic and equilibrium constants were determined. Line strengths were calculated from an ab initio transition-dipole moment function scaled using an experimental lifetime. A new line list for $v' = 0$–2 and $v'' = 0$–4 of the $B^3\Pi - X^3\Delta$ band system is provided.

Unified Astronomy Thesaurus concepts: Laboratory astrophysics (2004); Spectral line lists (2082)

Supporting material: machine-readable tables

1. Introduction

The TiO molecule has a long and significant astronomical history. Its fluted spectral lines were noted by Fowler (1907) in the spectra of Antarian stars, and its spectrum has been used as part of the Morgan Keenan (MK) classification system (Morgan & Keenan 1973). For M dwarf stars, the most numerous star type in our galaxy, the spectra are marked with strong absorption features due to TiO (Bochanski et al. 2007).

The near-IR and visible electronic transition spectra of TiO have been explored in sunspots (Ram et al. 1999) and in embedded protostars (Hillenbrand et al. 2012). The pure rotational microwave transitions of TiO have been detected in red supergiants, supporting the concept that titanium oxides are formed in circumstellar envelopes and seed inorganic dust formation (Kamiński et al. 2013). Its importance continues to expand as we explore exoplanets, where it has been detected by its electronic spectra and shown to cause formation of stratospheres in hot Jupiters (Evans et al. 2016; Nugroho et al. 2017).

TiO is particularly important as a strong source of opacity in the visible and near-IR (McKemmish et al. 2017). Therefore, accurate TiO line lists are essential in successfully modeling the spectra of many astronomical objects. The current ExoMol line list for TiO (McKemmish et al. 2019) remains the most reliable overall. Instead of using a Hamiltonian approach based on spectroscopic constants as this research does, the ExoMol line list is generated from potential energy curves using the DUO program (Yurchenko et al. 2016). The line list contains the $^{46}Ti^{16}O$, $^{47}Ti^{16}O$, $^{48}Ti^{16}O$, $^{49}Ti^{16}O$, and $^{50}Ti^{16}O$ isotopologues of TiO with 30 million transitions for $^{48}Ti^{16}O$. Laboratory spectroscopy is essential in the continuing effort to expand and improve the TiO line list.

A good recent summary of the state of laboratory spectroscopy of TiO research is provided by McKemmish et al. (2017). Efforts taken by our group since that summary include a reanalysis of the TiO singlet transitions (Bittner & Bernath 2018), the $C^3\Delta - X^3\Delta$ transition (Hodges & Bernath 2018), high-resolution absorption cross sections in the visible and near-IR (Bernath 2020a), and the $E^3\Pi - X^3\Delta$ transition in the near-IR (Bernath & Cameron 2020).

The $B^3\Pi - X^3\Delta$ transition (γ' system) contains strong lines and is a dominant feature of late-type stars (Hocking et al. 1979). The $B - X$ 0–0, 1–0, 0–1, and 1–1 bands were previously studied by emission spectroscopy, revealing significant lambda doubling in the $B^3\Pi$ state, and provided molecular constants for the $v = 0$ and $v = 1$ levels of the $B^3\Pi$ and $X^3\Delta$ states (Hocking et al. 1979). The $B - X$ 1–0 band was revisited and updated by the laser spectroscopy of a molecular beam (Amiot et al. 1995). Through Stark spectroscopy, the permanent electric dipole moments of the $B^3\Pi_0$ and $X^3\Delta_1$ states along with the $E^3\Pi_0$ and $A^3\Phi_2$ were measured (Steimle & Virgo 2003). The IR spectrum of $^{46-50}TiO$ was measured around 1000 cm^{-1} using a laser ablation source probed by IR radiation produced by quantum cascade lasers (Witsch et al. 2021).

The starting point for our $B^3\Pi - X^3\Delta$ analysis is the study of the $A^3\Pi - X^3\Delta$ system by Ram et al. (1999), which provided the equilibrium constants for the $X^3\Pi$ state, the spectroscopic constants for $v = 0$–4 of the X state, and the constants for $v = 1$ of the B state. The data were obtained from laboratory and sunspot spectra recorded using a Fourier transform spectrometer.

2. Method and Results

The TiO experimental cross sections (Bernath 2020a) used in this analysis are based on the same emission spectrum recorded at the McMath-Pierce Solar Telescope using the the 1 m Fourier transform spectrometer operated by the National Solar Observatory at Kitt Peak, Arizona that was used by Bernath & Cameron (2020) for their $E^3\Pi - X^3\Delta$ work. The source, a carbon tube furnace operating at about 2300 K, and the method of conversion of the emission spectrum to calibrated cross sections are described in detail by Bernath (2020a). The spectral resolution is about 0.05 cm^{-1} with wavenumber calibration accuracy ±0.002 cm^{-1}. Figure 1 shows the cross sections in red pointing upwards with the simulation pointing downwards showing the $B^3\Pi - X^3\Delta$ 0–0, 1–0, and 2–1 bands (green) and the $A^3\Phi - X^3\Delta$ 2–0 band (blue).

The $B^3\Pi$ and $X^3\Delta$ states obey Hund's case (a) coupling. The $B - X$ transition has three spin components: $B^3\Pi_2 - X^3\Delta_3$, $B^3\Pi_1 - X^3\Delta_2$, and $B^3\Pi_0 - X^3\Delta_1$. The state labels of the spin components are for $^3\Pi$: $F_3 = {}^3\Pi_2$, $F_2 = {}^3\Pi_1$, $F_1 = {}^3\Pi_0$; the

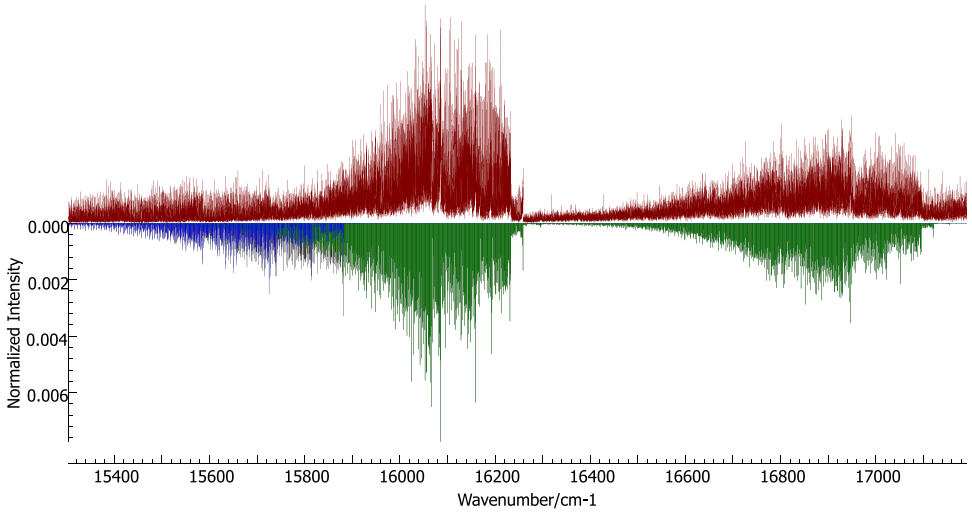

Figure 1. TiO spectrum in red pointing upwards, simulation pointing downwards showing the 2–0 $A^3\Phi - X^3\Delta$ band in blue and the 0–0, 1–0, and 2–1 $B^3\Pi - X^3\Delta$ bands in green. The $B^3\Pi - X^3\Delta$ 0–0 band is to the left, running from about 15800–16200 cm^{-1}; the 1–0 and 2–1 bands are intermixed to the right, running from about 16200–17100 cm^{-1}.

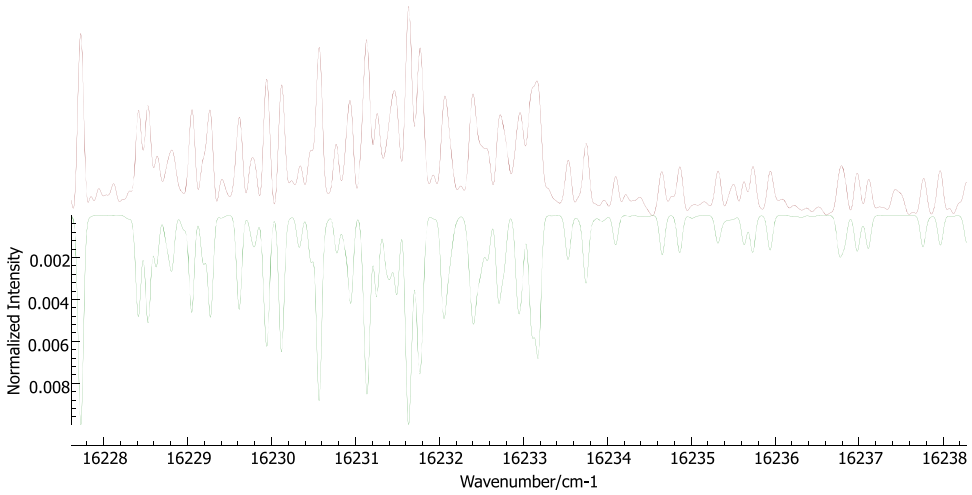

Figure 2. TiO $B^3\Pi - X^3\Delta$ spectrum in red pointing upwards, simulation pointing downwards in green, showing the 0–0 R_{1e} bandhead at about 16233.2 cm^{-1} and the 0–0 R_{1f} bandhead at about 16231.8 cm^{-1}.

Table 1
R Bandhead Locations for the TiO $B^3\Pi - X^3\Delta$ Transition

Transition	Bandhead	0–0 (cm^{-1})	1–0 (cm^{-1})	2–1 (cm^{-1})
$B^3\Pi_{0^+} - X^3\Delta_1$	R_{1e}	16233.19	17096.31	16957.91
$B^3\Pi_{0^-} - X^3\Delta_1$	R_{1f}	16231.79	17095.00	16956.66
$B^3\Pi_1 - X^3\Delta_2$	R_{2e}	16160.04	17023.30	16885.39
$B^3\Pi_1 - X^3\Delta_2$	R_{2f}	16160.23	17023.50	16885.62
$B^3\Pi_2 - X^3\Delta_3$	R_{3e}	16085.46	16947.29	16809.36
$B^3\Pi_2 - X^3\Delta_3$	R_{3f}	16085.87	16947.59	16809.60

following are for $^3\Delta$: $F_3 = {}^3\Delta_3$, $F_2 = {}^3\Delta_2$, and $F_1 = {}^3\Delta_1$ (Bernath 2020b). Each sub-band has P, Q, and R branches, and each branch has "e" and "f" parities due to lambda doubling. The R-branch bandheads for the 0–0, 1–0, and 2–1 bands of the $B^3\Pi - X^3\Delta$ transition are listed in Table 1. Figure 2 shows the $B^3\Pi_0 - X^3\Delta_1$ R bandheads.

The PGOPHER program (Western 2017) was used to perform the rotational analysis of the TiO $B - X$ transition. The process started with $B^3\Pi$ equilibrium constants from Amiot et al. (2002), which were used to calculate case (a) v state constants for $v = 0$ through $v = 4$, using Ram et al. (1999) $v = 1$ constants as a benchmark. For the $X^3\Delta$ constants, Ram et al. (1999) was again used. Ram et al. (1999) improved the existing ground state constants by combining sunspot and laboratory spectra with the pure rotational measurement of Steimle et al. (1990) and Namiki et al. (1998). The cross section file was used as an overlay in PGOPHER. Spectroscopic constants were updated as lines were fit up to J of at least 100. Attempts were made to fit lines in the 3–2 band, but the region of the spectrum was so congested the fit was not deemed reliable. In the rotational analysis, 5507 lines were fitted with an average error of 0.024 cm^{-1}. The TiO line database presented by McKemmish et al. (2019) includes the five stable isotopologues: $^{46}Ti^{16}O$, $^{47}Ti^{16}O$, $^{48}Ti^{16}O$, $^{49}Ti^{16}O$, and $^{50}Ti^{16}O$. The telluric abundances of ^{46}Ti, ^{47}Ti, ^{48}Ti, ^{49}Ti, and ^{50}Ti are 8.25%, 7.44%, 73.72%, 5.41%, and 5.18% respectively (Meija et al. 2016). The minor isotopologues are clearly present in the experimental spectrum from Kitt Peak but did not complicate the analysis of the most abundant isotopologue. Rotational analysis of the four minor isotopologues of TiO is a topic of our ongoing research. New spectroscopic constants resulting from

Table 2
Spectroscopic Constants for the $v = 0$ through $v = 2$ Levels of the $B^3\Pi$ State in cm^{-1}

Constant	$v = 0$	$v = 1$	$v = 1$(Ram et al. 1999)	$v = 2$
T_v	16148.4377(16)	17012.4714(14)	17012.463041(147)	17874.6285(14)
B_v	0.5060425(16)	0.50286131(71)	0.502865409(228)	0.49966314(81)
$D_v \times 10^7$	6.8913(41)	6.89443(93)	6.90626(113)	6.4812(13)
$H_v \times 10^{14}$	7.4(29)	0.84(33)	9.82(142)	−2153.09(59)
A_v	20.3851(21)	20.7817(21)	20.788469(223)	21.2050(20)
$A_{Dv} \times 10^4$	−1.65(28)	0.47(19)	−1.1437(257)	−2.41(22)
$A_{Hv} \times 10^9$	−6.51(43)	−6.26(12)	−6.446(105)	−4.96(35)
$\gamma_v \times 10^2$	2.333(56)	2.819(40)	2.49139(521)	2.2831(471)
λ_v	−0.7900(23)	−0.9329(23)	−0.93069(235)	−1.0733(22)
$\lambda_{Dv} \times 10^5$	−0.099(61)	−1.147(33)	−0.3826(658)	2.21(14)
$\lambda_{Hv} \times 10^8$	⋯	⋯	−0.0519(161)	−1.8761(88)
o_v	−0.6582(21)	−0.6139(22)	−0.618623(260)	−0.5800(24)
$o_{Dv} \times 10^6$	4.74(93)	−4.91(97)	1.918(427)	12.2(13)
$o_{Hv} \times 10^{10}$	⋯	5.14(53)	⋯	−19.53(98)
$p_v \times 10^2$	2.5573(65)	2.6156(67)	2.611711(933)	2.7552(81)
$p_{Dv} \times 10^8$	8.80(91)	6.4(13)	⋯	29.9(22)
$p_{Hv} \times 10^{12}$	⋯	3.58(63)	⋯	−3.6(14)
$q_v \times 10^4$	2.909(18)	3.062(11)	2.95986(352)	3.050(14)
$q_{Dv} \times 10^{10}$	−3.6(14)	−6.88(41)	⋯	−223.75(77)

Note. Numbers in parentheses are uncertainties to 1 standard deviation.

Table 3
Equilibrium Constants for the $B^3\Pi$ State in cm^{-1}

Constant	New Values	(Amiot et al. 2002)
ω_e	865.91124	865.87593
$\omega_e x_e$	0.93876	0.924582159
B_e	0.50762697	0.50763(388)
$\alpha_e \times 10^3$	3.16477	3.179246
$\gamma_e \times 10^6$	−8.23	⋯

the rotational analysis for $v = 0$ though $v = 2$ of the B state are provided in Table 2. The reader may note the H_v value for $v = 2$ appears to be anomalous; thorough investigation of the constant through PGOPHER shows it to be stable with small relative standard deviation. Higher-order lambda-doubling centrifugal distortion terms were statistically determined for the B state due to large lambda doubling in the $B - X$ transition. It is possible global perturbations exist, but no local perturbations were discovered. The standard N^2 Hamiltonian (Ram et al. 1999) was used for fitting.

New equilibrium constants are provided in Table 3. The equilibrium constants were derived by the exact fit of the PGOPHER generated spectroscopic constants. The number of decimal places shown in the equilibrium constants was determined by allowing a ±1 standard deviation in the value of the spectroscopic constants. The equilibrium constants were input into Le Roy's Rydberg-Klein-Rees (RKR) program (Le Roy 2017a) to generate the potential energy curves for the B and X states, which were then inserted into Le Roy's LEVEL program (Le Roy 2017b), along with the transition-dipole moment points, to generate transition-dipole moment matrix elements. The transition-dipole moment points for the $B - X$ transition were obtained from McKemmish et al. (2019), who fit a curve to their own ab initio data as well as the ab initio data of Langhoff (1997). The functional form of the fit for the transition-dipole μ is

$$\mu_{\text{fit}}(r) = \frac{c}{2\pi}(\pi + 2\tan^{-1}(-a(r - r_m))), \quad (1)$$

in which c, a, and r_m are fitting parameters; for the $B - X$ transition, $c = 5.013$, $a = 4.101$ and $r_m = 1.667$. Excel was used to calculate 317 transition-dipole moment points for $r = 0.84$–2.42 Å.

Table 4
Scaled Transition-dipole Moment Matrix Elements for the $B^3\Pi - X^3\Delta$ Transition in Debye

Band $v' - v''$	Transition-dipole Moment Matrix Element (debye)
0–0	3.08127
1–0	−2.01087
2–0	0.93507
0–1	1.44348
1–1	2.03017
2–1	−2.32573
0–2	0.46731
1–2	1.69027
2–2	1.15678
0–3	0.12070
1–3	0.71320
2–3	1.69059
0–4	$2.40917x10^{-2}$
1–4	0.218792
2–4	0.885716

The average radiative lifetime of the three spin states of the $v = 0$ B state was measured to be 65.4 ± 1.3 ns (Hedgecock et al. 1995). The Einstein A for the $v = 0$ B state can be calculated, with the calculated lifetime τ for the state being

$$\tau = \frac{1}{\sum A_{0\to v''}}. \quad (2)$$

Table 5
Sample of Fitted Lines for the $B^3\Pi - X^3\Delta$ Transition Based on the PGOPHER Log File

J'	p'	J''	p''	Obs (cm^{-1})	Calc (cm^{-1})	O-C (cm^{-1})	Line	Line Assignment
3	f	3	e	16225.3072	16225.3166	−0.0094	qQ1e(3)	B v = 0 3 2 F1f—X v = 0 3 2 F1e
4	f	4	e	16224.9672	16224.9628	0.0044	qQ1e(4)	B v = 0 4 3 F1f—X v = 0 4 3 F1e
5	e	5	f	16793.445	16793.43	0.015	qQ3f(5)	B v = 2 5 6 F3e—X v = 1 5 6 F3f
62	e	62	f	16890.5924	16890.5999	−0.0075	qQ2f(62)	B v = 1 62 62 F2e—X v = 0 62 62 F2f
10	e	11	e	16210.8103	16210.8135	−0.0032	pP1e(11)	B v = 0 10 9 F1e—X v = 0 11 10 F1e
85	f	86	f	16545.7223	16545.7023	0.02	pP2f(86)	B v = 2 85 85 F2f—X v = 1 86 86 F2f
11	f	10	f	16077.8369	16077.8404	−0.0035	rR3f(10)	B v = 0 11 12 F3f—X v = 0 10 11 F3f
102	f	101	f	16829.3663	16829.3996	−0.0333	rR1f(101)	B v = 1 102 101 F1f—X v = 0 101 100 F1f

Note. J is total angular momentum; p is the e/f parity; Obs is the observed line position in cm^{-1}; Calc is the calculated line position in cm^{-1}; O-C is the observed-minus-calculated line position in cm^{-1}; Line is the spectroscopic line label; Line assignment contains additional information.

(This table is available in its entirety in machine-readable form.)

Table 6
Sample Line List for the $B^3\Pi - X^3\Delta$ Transition of TiO

J'	J''	Pos (cm^{-1})	Eup (cm^{-1})	Elow (cm^{-1})	A (s^{-1})	f	Line	Line assignment
21	20	17022.517	17245.485	222.968	8.922E+05	4.841E-03	rR2f(20)	B v = 1 21 21 F2f—X v = 0 20 20 F2f
10	9	17022.522	17069.345	46.823	9.208E+05	5.265E-03	rR2e(9)	B v = 1 10 10 F2e—X v = 0 9 9 F2e
28	28	17022.572	17454.600	432.027	6.563E+05	3.395E-03	rQ32f(28)	B v = 1 28 29 F3e—X v = 0 28 28 F2f
20	19	17022.582	17224.206	201.624	9.027E+05	4.910E-03	rR2e(19)	B v = 1 20 20 F2e—X v = 0 19 19 F2e
57	58	17022.588	18726.276	1703.689	1.273E+04	6.474E-05	rP31e(58)	B v = 1 57 58 F3e—X v = 0 58 57 F1e
10	9	17022.646	17069.470	46.823	9.197E+05	5.259E-03	rR2f(9)	B v = 1 10 10 F2f—X v = 0 9 9 F2f
41	41	17022.704	17832.655	809.950	2.486E+06	1.286E-02	qQ1f(41)	B v = 1 41 40 F1e—X v = 0 41 40 F1f
11	10	17022.800	17080.303	57.503	9.337E+05	5.291E-03	rR2e(10)	B v = 1 11 11 F2e—X v = 0 10 10 F2e

Note. J is total angular momentum; Pos is the line position in vacuum cm^{-1}; Eup and Elow are upper and lower energy levels in cm^{-1}; A is Einstein A value in s^{-1}; f is the oscillator strength; Line is the spectroscopic line label.

(This table is available in its entirety in machine-readable form.)

The Einstein A is linked to line strength through the following relationship:

$$A_{v'\rightarrow v''} = 3.136189 \times 10^{-7}\tilde{\nu}^3 S_{v'\rightarrow v''} \quad (3)$$

where $\tilde{\nu}$ is in cm^{-1} (Bernath 2020b). The line strength S is the square of the transition-dipole moment. The transition-dipole moment matrix elements were obtained from the LEVEL program. Comparing the calculated radiative lifetime of 122.3 ns to the measured radiative lifetime shows that a correction factor of 1.87 must be applied to the calculated Einstein A values. The calculated transition-dipole moment matrix elements obtained from the LEVEL program were corrected by applying a scaling factor of $\sqrt{1.87}$ to make this correction to the PGOPHER band strengths. Based on the experimental accuracy of 2.0% for the lifetime of $v = 0$ (Hedgecock et al. 1995), the minimum error for calculated Einstein A values is also about 2%. The scaled transition-dipole moment matrix elements are shown in Table 4.

3. Discussion

The spectroscopic constants (Table 2) extend the previously published $v' = 1$ constants of Ram et al. (1999) to also include $v' = 0$ and $v' = 2$. A sample of the lines fitted and the observed-minus calculated values are given in Table 5. Table 5 uses the traditional spectroscopic line label: ${}^{\Delta N}\Delta J_{F_i' F'' j} p(J)$ where N is the quantum number for the total angular momentum excluding electron spin, J is the quantum number for the total angular momentum, p is the e/f rotationless parity, and F_i is the spin component label discussed in the previous section. In addition, the line assignment information in Table 5 uses the PGOPHER *NameJNFnp* format.

Through this analysis, the equilibrium constants (Table 3) of the $B^3\Pi$ state (Amiot et al. 2002) have also been updated. McKemmish et al. (2019) noted that future improvements on the TiO line list should concentrate on wavelength regions such as 570–640 nm (15625–17544 cm^{-1}), which is coincident with the $B^3\Pi - X^3\Delta$ 0–0, 1–0, and 2–1 bands that are the focus of this research. Using the $X^3\Delta$ spectroscopic constants for $v'' = 0$ through $v'' = 4$ from Ram et al. (1999) and the new $B^3\Pi$ spectroscopic constants from Table 2, a new line list for the $B^3\Pi - X^3\Delta$ transition has been calculated; a sample of that line list is shown in Table 6. The same line and line assignment formats used in Table 5 are used in Table 6.

The transition-dipole moment matrix elements shown in Table 4 were used in PGOPHER as band strengths to obtain a more complete line list. In addition, the oscillator strength for each line, $f_{J'\leftarrow J''}$, was calculated from the Einstein A values, which are provided for each line by PGOPHER, using the following:

$$f_{J'\leftarrow J''} = \frac{\epsilon_0 m_e c^3}{2\pi e^2 \nu^2}\frac{2J'+1}{2J''+1}A_{J'\rightarrow J''}, \quad (4)$$

where SI units are used. In terms of numerical values, the equation becomes

$$f_{J'\leftarrow J''} = \frac{1.499194}{\tilde{\nu}^2}\frac{2J'+1}{2J''+1}A_{J'\rightarrow J''}, \quad (5)$$

with $\tilde{\nu}$ in cm^{-1} (Bernath 2020b).

The line list was compared with both the ExoMol line list and Amiot et al. (1995). As noted by Bernath (2020a), the 0–0 band in the ExoMol line list agrees well with the measured cross sections down to about 16200 cm^{-1}, below that wavenumber missing/shifted lines and intensity errors begin to appear. 16200 cm^{-1} marks the upper (low J) end of the 0–0 band. A slightly more detailed analysis shows occasional errant lines from 16200 down to about 16050 cm^{-1} at which point they become more commonplace, roughly around $J = 60$. The 0–0 band is the ideal comparison between this research and the ExoMol line list in that it is somewhat isolated as opposed to the region where the 1–0, 2–1, and 3–2 bands are mostly overlaid, making unique line identification often challenging. From about 17100 cm^{-1} down to about 17000 cm^{-1}, the 1–0 band is relatively isolated; J values are typically below 60, and both the line list generated here and the ExoMol line list are in good agreement with the measured cross sections. Comparing the line list from this research with the Amiot et al. (1995) line list, which encompasses the 1–0 band from $J = 1$–100, a subset from all three branches, both the parities and J values ranging from 5 to 100 show an average difference of less than 0.005 cm^{-1}.

4. Conclusion

The new TiO $B^3\Pi - X^3\Delta$ line list derived from the TiO emission spectrum recorded at the McMath-Pierce Solar Telescope, operated by the National Solar Observatory at Kitt Peak, Arizona in 1985 January (Bernath 2020a) improves on the existing data. New spectroscopic constants for $v' = 0$–2 in the B state have been produced, expanding the existing constants from Ram et al. (1999) and updating the equilibrium constants from Amiot et al. (1995). The fitted lines and the calculated line list for $v' = 0$–2 and $v'' = 0$–4, sampled in Tables 5 and 6 respectively, are available in their entirety as supplementary data files.

The National Solar Observatory (NSO) is operated by the Association of Universities for Research in Astronomy, Inc. (AURA), under cooperative agreement with National Science Foundation. Financial support was provided by the NASA Exoplanet Research Program (80NSSC21K0412).

Software: PGOPHER (Western 2017), Excel.

ORCID iDs

Peter Bernath https://orcid.org/0000-0002-1255-396X

References

Amiot, C., Azaroual, E. M., Luc, P., & Vetter, R. 1995, JChPh, 102, 4375
Amiot, C., Luc, P., & Vetter, R. 2002, JMoSp, 214, 196
Bernath, P. 2020a, ApJ, 895, 87
Bernath, P., & Cameron, W. D. 2020, ApJ, 904, 24
Bernath, P. F. 2020b, Spectra of Atoms and Molecules (Oxford: Oxford Univ. Press)
Bittner, D. M., & Bernath, P. F. 2018, ApJS, 236, 46
Bochanski, J. J., West, A. A., Hawley, S. L., & Covey, K. R. 2007, AJ, 133, 531
Evans, T. M., Sing, D. K., Wakeford, H. R., et al. 2016, ApJL, 822, L4
Fowler, A. 1907, RSPSA, 79, 509
Hedgecock, I., Naulin, C., & Costes, M. 1995, A&A, 304, 667
Hillenbrand, L. A., Knapp, G. R., Padgett, D. L., Rebull, L. M., & McGehee, P. M. 2012, AJ, 143, 37
Hocking, W. H., Gerry, M., & Merer, A. 1979, CaJPh, 57, 54
Hodges, J. N., & Bernath, P. F. 2018, ApJ, 863, 36
Kamiński, T., Gottlieb, C., Menten, K., et al. 2013, A&A, 551, A113
Langhoff, S. R. 1997, ApJ, 481, 1007
Le Roy, R. J. 2017a, JQSRT, 186, 158
Le Roy, R. J. 2017b, JQSRT, 186, 167
McKemmish, L. K., Masseron, T., Hoeijmakers, H. J., et al. 2019, MNRAS, 488, 2836
McKemmish, L. K., Masseron, T., Sheppard, S., et al. 2017, ApJS, 228, 15
Meija, J., Coplen, T. B., Berglund, M., et al. 2016, Pure Appl. Chem., 88, 265
Morgan, W. W., & Keenan, P. 1973, ARA&A, 11, 29
Namiki, K.-I., Saito, S., Robinson, J. S., & Steimle, T. C. 1998, JMoSp, 191, 176
Nugroho, S. K., Kawahara, H., Masuda, K., et al. 2017, AJ, 154, 221
Ram, R., Bernath, P., Dulick, M., & Wallace, L. 1999, ApJS, 122, 331
Steimle, T., Shirley, J., Jung, K., Russon, L., & Scurlock, C. 1990, JMoSp, 144, 27
Steimle, T. C., & Virgo, W. 2003, CPL, 381, 30
Western, C. M. 2017, JQSRT, 186, 221
Witsch, D., Breier, A. A., Döring, E., et al. 2021, JMoSp, 377, 111439
Yurchenko, S. N., Lodi, L., Tennyson, J., & Stolyarov, A. V. 2016, CoPhC, 202, 262